BIOCHEMISTRY
including biophysical chemistry & molecular biology
Article

Biochemistry **2009,** *48,* 4331–4343 4331
DOI:10.1021/bi900109z

Substrate-Triggered Formation and Remarkable Stability of the C−H Bond-Cleaving Chloroferryl Intermediate in the Aliphatic Halogenase, SyrB2[†]

Megan L. Matthews,[‡] Courtney M. Krest,[‡] Eric W. Barr,[§] Frédéric H. Vaillancourt,[∥,⊥] Christopher T. Walsh,*[,∥] Michael T. Green,*[,‡] Carsten Krebs,*[,‡,§] and J. Martin Bollinger, Jr.*[,‡,§]

[‡]*Department of Chemistry and* [§]*Department of Biochemistry and Molecular Biology, The Pennsylvania State University, University Park, Pennsylvania 16802, and* [∥]*Department of Biological Chemistry and Molecular Pharmacology, Harvard Medical School, 240 Longwood Avenue, Boston, Massachusetts 02115* [⊥]*Present address: Boehringer Ingelheim Ltd., Laval, QC, Canada*

Received January 23, 2009; Revised Manuscript Received February 25, 2009

ABSTRACT: Aliphatic halogenases activate O_2, cleave α-ketoglutarate (αKG) to CO_2 and succinate, and form haloferryl [X−Fe(IV)═O; X = Cl or Br] complexes that cleave aliphatic C−H bonds to install halogens during the biosynthesis of natural products by non-ribosomal peptide synthetases (NRPSs). For the related αKG-dependent dioxygenases, it has been shown that reaction of the Fe(II) cofactor with O_2 to form the C−H bond-cleaving ferryl complex is "triggered" by binding of the target substrate. In this study, we have tested for and defined structural determinants of substrate triggering (ST) in the halogenase, SyrB2, from the syringomycin E biosynthetic NRPS of *Pseudomonas syringae* B301D. As for other halogenases, the substrate of SyrB2 is complex, consisting of L-Thr tethered via a thioester linkage to a covalently bound phosphopantetheine (PPant) cofactor of a carrier protein, SyrB1. Without an appended amino acid, SyrB1 does not trigger formation of the chloroferryl intermediate state in SyrB2, even in the presence of free L-Thr or its analogues, but SyrB1 charged either by L-Thr (L-Thr-*S*-SyrB1) or by any of several non-native amino acids does trigger the reaction by as much as 8000-fold (for the native substrate). Triggering efficacy is sensitive to the structures of both the amino acid and the carrier protein, being diminished by 5−24-fold when the native L-Thr is replaced with another amino acid and by ∼40-fold when SyrB1 is replaced with the heterologous carrier protein, CytC2. The directing effect of the carrier protein and consequent tolerance for profound modifications to the target amino acid allow the chloroferryl state to be formed in the presence of substrates that perturb the ratio of its two putative coordination isomers, lack the target C−H bond (L-Ala-*S*-SyrB1), or contain a C−H bond of enhanced strength (L-cyclopropylglycyl-*S*-SyrB1). For the latter two cases, the SyrB2 chloroferryl state so formed exhibits unprecedented stability ($t_{1/2}$ = 30−110 min at 0 °C), can be trapped at high concentration and purity by manual freezing without a cryosolvent, and represents an ideal target for structural characterization. As initial steps toward this goal, extended X-ray absorption fine structure (EXAFS) spectroscopy has been used to determine the Fe−O and Fe−Cl distances and density functional theory (DFT) calculations have been used to confirm that the measured distances are consistent with the anticipated structure of the intermediate.

The Fe(II)- and α-ketoglutarate-dependent oxygenases activate O_2 at mononuclear non-heme Fe(II) centers to catalyze hydroxylation, desaturation, cyclization, and isomerization reactions (*1*−*4*). In each case, the two-electron oxidation of the substrate is coupled to oxidative decarboxylation of the cosubstrate, α-ketoglutarate (αKG),[1] to CO_2 and succinate, providing the two additional reducing equivalents needed to balance the four-electron reduction of O_2. In the most extensively studied members of the family, the Fe(II) cofactors are similarly coordinated by a conserved $(His)_2(Asp/Glu)$ "facial triad" of protein ligands (*5*, *6*). Bidentate coordination of αKG leaves

[†]This work was supported by the National Institutes of Health (GM-20011 and GM-49338 to C.T.W. and GM-69657 to J.M.B. and C.K.), the National Science Foundation (MCB-642058 to J.M.B. and C.K. and MCB-47676 to M.T.G.), the Beckman Foundation (Young Investigator Awards to M.T.G. and C.K.), the Dreyfus Foundation (Teacher-Scholar Award to C.K.), and Merck via the Helen Hay Whitney Foundation and the Natural Sciences and Engineering Research Council of Canada (postdoctoral fellowships to F.H.V.). Portions of this research were carried out at the Stanford Synchrotron Radiation Lightsource, a national user facility operated by Stanford University on behalf of the U.S. Department of Energy, Office of Basic Energy Sciences. The SSRL Structural Molecular Biology Program is supported by the Department of Energy, Office of Biological and Environmental Research, and by the National Institutes of Health, National Center for Research Resources, Biomedical Technology Program.

* To whom correspondence should be addressed. J.M.B.: Department of Chemistry, 336 Chemistry Building, University Park, PA 16802; phone, (814) 863-5707; fax, (814) 865-2927; e-mail, jmb21@psu.edu. C.K.: Department of Chemistry, 332 Chemistry Building, University Park, PA 16802; phone, (814) 865-6089; fax, (814) 865-2927; e-mail, ckrebs@psu.edu. M.T.G.: Department of Chemistry, 331 Chemistry Building, University Park, PA 16802; phone, (814) 863-0925; fax, (814) 865-2927; e-mail, mtg10@psu.edu. C.T.W.: Department of Biological Chemistry and Molecular Pharmacology, 240 Longwood Ave., Boston, MA 02115; phone, (617) 432-1715; fax, (617) 432-0438; e-mail, christopher_walsh@hms.harvard.edu.

Published on Web 2/26/2009

Scheme 1: HAG Mechanism (*10*) for the Fe(II)- and αKG-Dependent Hydroxylases (A) and Hypothesis for How the Hydroxylase and Halogenase Mechanisms Diverge (B) (*22*)

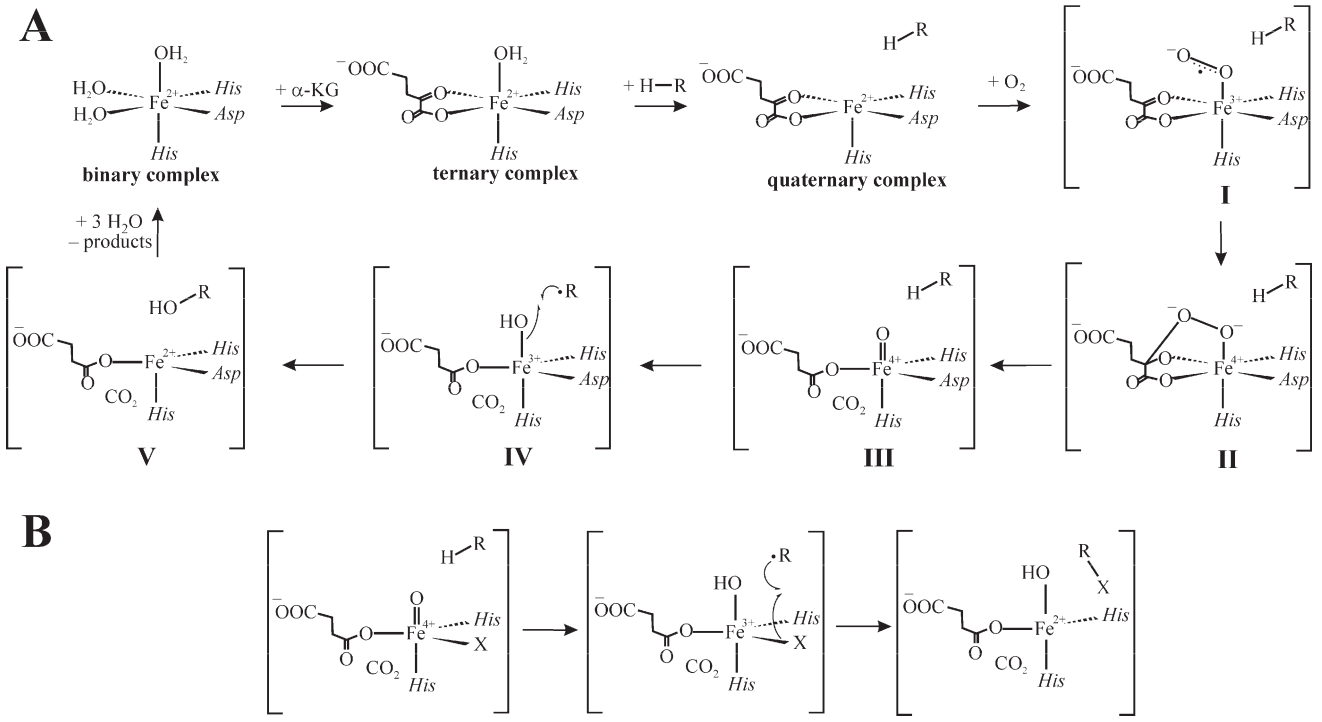

one remaining position in the octahedral coordination sphere to which O_2 can add to be activated (*2*, *7*, *8*). As first proposed by Hanauske-Abel and Günzler [in what the first author later termed the "HAG" mechanism (*9*)], this step leads to formation of a hydrogen-abstracting iron(IV)−oxo (ferryl) intermediate (Scheme 1A) (*10*). In the reactions of two family members, taurine:αKG dioxygenase (TauD) and a prolyl-4-hydroxlase (P4H) from *Paramecium bursaria* Chlorella virus 1 (PBCV-1), the ferryl complexes have been directly demonstrated (*11*, *12*). The kinetics of the ferryl intermediates were monitored in stopped-flow experiments by their ultraviolet absorption (at ~320 nm) and in freeze-quench Mössbauer experiments by their quadrupole doublets with small isomer shifts (~0.3 mm/s). Large substrate deuterium kinetic isotope effects ([^{2}H]KIEs) on decay of the intermediates (k_H/k_D = 50−60) showed that they both abstract hydrogen (*12*, *13*). The TauD intermediate was further characterized by resonance Raman (rR) (*14*) and extended X-ray absorption fine structure (EXAFS) spectroscopy (*15*), which confirmed the presence of the Fe=O unit. According to the HAG mechanism, the ferryl complex abstracts a hydrogen atom (H•), and subsequent "rebound" (*16*) of a hydroxyl radical equivalent from the resultant Fe(III)−OH complex to the substrate radical yields the hydroxylated product and Fe(II) form of the cofactor (Scheme 1A) (*10*).

SyrB2 from the syringomycin E biosynthetic system in *Pseudomonas syringae* B301D (Scheme 2A) was recently characterized as the founding member of a subfamily of αKG-dependent oxygenases that effect oxidative halogenation (mono- and dichlorination and bromination) of unactivated carbon centers in the biosyntheses of natural products by non-ribosomal peptide synthetases (NRPSs) (*17*−*21*). The structure of the enzyme determined by X-ray crystallography revealed the carboxylate ligand from the canonical facial triad to be absent, replaced in the protein sequence by a noncoordinating alanine and in the Fe(II) coordination sphere by a halide ion (*22*). A mechanism derived from the HAG dioxygenase mechanism was proposed for SyrB2 and other aliphatic halogenases (Scheme 1B). The crucial features are, first, the formation of a haloferryl [X−Fe(IV)=O; X = Cl or Br] intermediate that abstracts H• from the substrate and, second, the rebound of the halogen atom, rather than the hydroxyl radical, from the resultant X−Fe(III)−OH complex to the substrate radical (*22*). The proposed C−H bond-cleaving intermediate was subsequently (i) detected in the reaction of the halogenase, CytC3 [from the cytotrienin A producer, *Streptomyces* sp. RK95-74 (Scheme 2B)], (ii) shown by the large substrate [^{2}H]KIE on its decay to abstract hydrogen, and (iii) demonstrated by EXAFS spectroscopy to have the expected X−Fe=O unit (for X = Br) (*23*, *24*). Interestingly, the haloferryl intermediate state was shown by Mössbauer spectroscopy to comprise two distinct Fe(IV) complexes, which were speculatively identified as rapidly interconverting coordination isomers. It was suggested that this isomerism could reflect conformational dynamics required for the alternative (halogen rather than hydroxyl) rebound (*23*).

An important characteristic of several (perhaps most) αKG-dependent oxygenases is "substrate triggering" (ST), a marked activation of the Fe(II) cofactor for reaction with O_2 caused by binding of the substrate (*1*−*3*). By disfavoring or preventing formation of the potently oxidizing ferryl complex until its oxidation target is in place, ST is thought to protect the enzyme against deleterious autoxidation reactions. For TauD, taurine

[1]Abbreviations: αKG, α-ketoglutarate; HAG, Hanauske-Abel and Günzler; TauD, taurine:αKG dioxygenase; P4H, prolyl-4-hydroxylase; PBCV-1, *P. bursaria* Chlorella virus 1; [^{2}H]KIE, deuterium kinetic isotope effect; rR, resonance Raman; EXAFS, extended X-ray absorption fine structure; H•, hydrogen atom; haloferryl, X−Fe(IV)=O (X = Cl or Br); ST, substrate triggering; 6C, six-coordinate; 5C, five-coordinate; PPant, phosphopantetheine; L-Aba, L-α-aminobutyric acid; DFT, density functional theory; XAS, X-ray absorption spectroscopy; A domain, adenylation domain; T domain, thiolation domain; BDE, homolytic bond dissociation energy.

Scheme 2: Reactions Catalyzed by the Fe(II)- and αKG-Dependent Halogenases SyrB2 (A) and CytC3 (B)

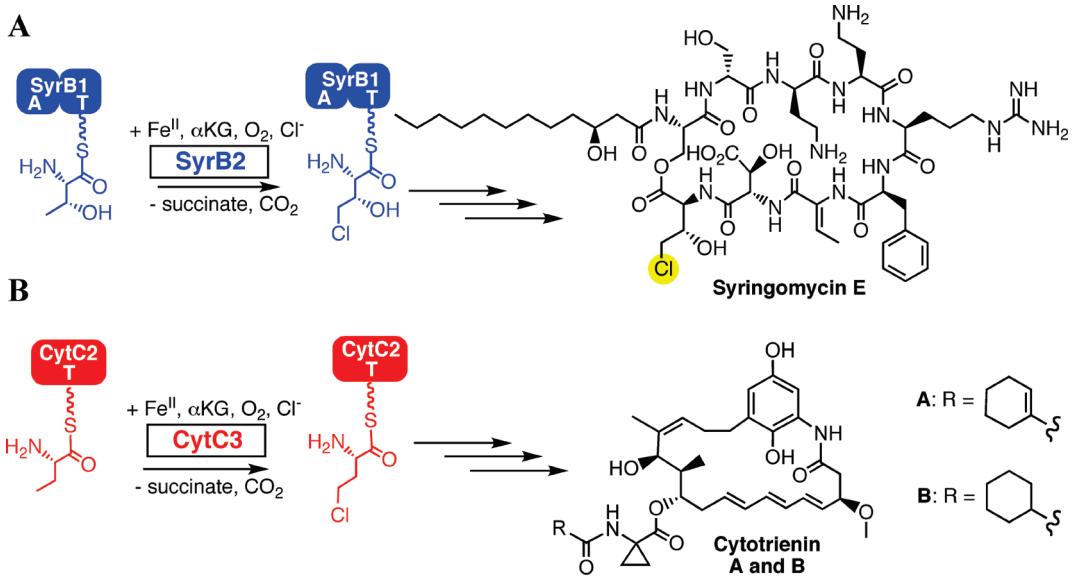

binding was shown to trigger the O_2 reaction by ~1000-fold (*25*, *26*). It is possible that the untriggered (lacking taurine) reaction might even proceed by a different mechanism, as no evidence could be obtained for accumulation of the ferryl complex under these conditions (*1*, *26*). Pioneering work of Solomon and co-workers showed first for clavaminate synthase and subsequently for other family members (including TauD) that conversion of the Fe(II) site from six-coordinate (6C) to five-coordinate (5C), making available the site to which O_2 adds, is at least partly responsible for the ST phenomenon (*2*, *7*, *8*, *27*). It is thought that a protein conformational change associated with substrate binding promotes dissociation of a water ligand, although the resultant 6C → 5C change may in some cases be incomplete (*8*). To the best of our knowledge, ST has not been systematically examined for the halogenases, although the partial 6C → 5C change upon addition of substrate was also observed for CytC3 (*8*). The substrate of a halogenase is complex and trimodular, consisting of an amino acid (L-Thr for the case of SyrB2) tethered via a thioester linkage to a phosphopantetheine (PPant) cofactor, which is in turn covalently attached via one of its Ser residues to a carrier protein (SyrB1) (Scheme 2) (*17*, *19*−*21*). In this study, we tested for ST in SyrB2, finding (i) that, indeed, reaction of the SyrB2·Fe(II)·αKG·Cl^- complex with O_2 is 8000 times faster in the presence of the native substrate (L-Thr-*S*-SyrB1) than in either the absence of the carrier protein or the presence of SyrB1 with its PPant module not charged by an amino acid (HS-SyrB1) and (ii) that only in the former case does the chloroferryl complex demonstrably accumulate. Contacts between the halogenase and both the carrier protein module and the amino acid module appear to contribute to ST, but forms of SyrB1 charged by a non-native amino acid still trigger by as much as ~1300-fold, and the L-Thr-charged form of the heterologous carrier protein, CytC2 (the carrier protein for the CytC3 halogenase), triggers by >300-fold. The tolerance for modifications to both terminal modules of the substrate affords several unique opportunities to explore the structure of the chloroferryl state, the nature of its conformational isomerism, and the mechanism by which it effects aliphatic chlorination. For example, variation of the amino acid is shown to allow the ratio of the two constituent complexes to be varied from ~4:1 for L-Thr-*S*-SyrB1 to ~1:5 for L-cyclopropylglycyl-*S*-SyrB1, a tool that should be useful for exploring the structural distinction between them by spectroscopy and computation. Conversely, use of the 10 kDa heterologous carrier protein, CytC2 (the carrier protein for CytC3), in place of the 66 kDa SyrB1 allows the O_2-reactive SyrB2·substrate complex, and thus potentially the chloroferryl intermediate, to be prepared at concentrations approaching the solubility of SyrB2 itself (>5 mM). Most importantly, the directing effect of the carrier protein permits the chloroferryl state to be formed with drastically modified amino acids that either lack the target C−H bond (L-Ala-*S*-SyrB1) or have a C−H bond of enhanced strength (L-cyclopropylglycyl-*S*-SyrB1). The SyrB2 chloroferryl state so formed is remarkably stable ($t_{1/2}$ = 30−110 min at 0 °C), can be trapped at high concentrations and purities by manual freezing without a cryo-solvent, and represents an ideal target for structural characterization. We use EXAFS spectroscopy on samples of the chloroferryl state prepared in this manner to obtain two crucial metrics, the Fe−O and Fe−Cl distances, for the SyrB2 intermediate. These metric parameters are consistent with those obtained by density functional theory (DFT) calculations.

MATERIALS AND METHODS

Materials. Yeast extract and tryptone were purchased from Marcor Development Corp. (Carlstadt, NJ). Isopropyl *β*-D-thiogalactopyranoside (IPTG) was purchased from Gold Biotechnology, Inc. (St. Louis, MO). Ethylenedinitrilotetraacetic acid (EDTA) disodium salt dihydrate and sodium chloride were purchased from EMD Chemicals, Inc. (Gibbstown, NJ). Kanamycin, phenylmethanesulfonyl fluoride (PMSF), 4-(2-hydroxyethyl)-1-piperazineethanesulfonic acid (HEPES), imidazole, coenzyme A, disodium adenosine 5′-triphosphate (ATP), α-ketoglutarate (αKG), ferrous ammonium sulfate hexahydrate, Ellman's reagent [5,5′-dithiobis(2-nitrobenzoic acid) (DTNB)], L-valine (L-Val), L-threonine (L-Thr), L-alanine (L-Ala), L-serine (L-Ser), and L-α-aminobutyric acid (L-Aba) were purchased from Sigma-Aldrich (St. Louis, MO) and used as received. Deoxyribonuclease (DNase) I and calcium chloride dihydrate were purchased from Fisher Scientific (Fair Lawn, NJ). Magnesium

chloride hexahydrate was purchased from J. T. Baker (Phillipsburg, N.J.). *Escherichia coli* BL21(DE3) cells were purchased from Gene Choice (San Diego, CA). ^{57}Fe metal was purchased from Advanced Materials and Technology, Inc. (New York, NY). It was converted to the $Fe(II)_{aq}$ form by dissolution of the metal in 2 N H_2SO_4, as previously described (*28*). 2,3,4,4,4-[^{2}H]$_5$-[^{15}N]-L-Threonine (d_5-L-Thr), 2,3,4,4,4,4′,4′-[^{2}H]$_8$-L-valine (d_8-L-Val), 3,3,3-[^{2}H]$_3$-L-alanine (d_3-L-Ala), and 2,3,3,4,4,4-[^{2}H]$_6$-L-α-aminobutyric acid (d_6-L-Aba) were purchased from Cambridge Isotope Laboratories, Inc. (Andover, MA). L-Cyclopropylglycine (L-Cpg) was kindly provided by Eastman Chemical Co. (Kingsport, TN). Ni(II)-nitrilotriacetic acid (Ni-NTA) agarose resin was purchased from Qiagen (Valencia, CA). Sephadex G-75 resin was purchased from Amersham Biosciences (Piscataway, NJ).

Overexpression and Purification of SyrB and CytC Proteins. Each protein used in this study, including SyrB2, SyrB1, CytC2, CytC1, and Sfp, has an additional 20 amino acids ($MGS_2H_6S_2GLVPRGSH$) appended to the N-terminal methionine residue. The appendage contains a His_6 element to permit purification of the protein by metal ion affinity chromatography on Ni-NTA agarose. Preparation of the plasmids that direct overexpression of these proteins in *E. coli*, growth of the overexpression strains, and purification of the proteins have been described previously (*17*, *29*, *30*). The overexpression and purification procedures have been adapted for purification in an aerobic environment, as described below.

Cultures of the overproducing strains were grown aerobically at 37 °C in rich LB broth [35 g/L tryptone, 20 g/L yeast extract, 5 g/L NaCl, and 0.05 g/L kanamycin (pH 7.0)] to an optical density at 600 nm of 0.6−0.8. They were cooled rapidly by incubation on ice for 30 min prior to addition of IPTG to a final concentration of 200 μM. Following induction, cultures were grown at 15−18 °C for an additional 16−18 h, and cells were harvested by centrifugation. The cell paste was flash-frozen in liquid N_2 and stored at −80 °C. A typical yield was ∼10−12 g of wet cell paste per liter of culture. The frozen cell paste was resuspended in 5 mL/g of 50 mM Na-HEPES buffer (pH 7.5) containing 300 mM NaCl, 5 mM imidazole, 0.25 mM PMSF, 0.1 mg/mL Dnase I, 1 mM $CaCl_2$, and 1 mM $MgCl_2$. The cells were lysed at 4 °C by a single passage through a French pressure cell at 16000 psi, and the resulting lysate was centrifuged at 10000*g* for 20 min. The supernatant was stirred gently with Ni-NTA resin (∼1 mL of resin per 5 mL of supernatant) for ∼30 min. The slurry was loaded into a column and washed with 50 mM Na-HEPES buffer (pH 7.5) containing 300 mM NaCl and 5 mM imidazole. Protein was eluted from the resin with 50 mM Na-HEPES (pH 7.5) containing 100 mM NaCl and 250 mM imidazole. Fractions containing the desired protein, as identified by denaturing polyacrylamide gel electrophoresis (SDS−PAGE) with Coomassie staining, were pooled and dialyzed against 20 mM Na-HEPES buffer (pH 7.5) (reaction buffer), supplemented with 1 mM EDTA. The protein was then dialyzed against two changes of reaction buffer lacking EDTA to remove the metal chelator. Following dialysis, all proteins were concentrated to ∼200 mg/mL prior to being flash-frozen and stored at −80 °C.

Determination of Protein Concentrations. The proteins were quantified spectrophotometrically by assuming molar absorptivities (ε_{280}) of 75290 M^{-1} cm^{-1} for SyrB1 (68307 Da), 59610 M^{-1} cm^{-1} for SyrB2 (37523 Da), 29130 M^{-1} cm^{-1} for Sfp (31684 Da), 5500 M^{-1} cm^{-1} for CytC2 (11585 Da), and 68090 M^{-1} cm^{-1} for CytC1 (58921 Da) as calculated by the method of Gill and von Hippel (*31*).

Substrate Assembly: Phosphopantetheinylation of the Carrier Protein and Charging of Amino Acids onto the PPant Cofactor. Phosphopantetheinylation of the purified apo forms of both carrier proteins (CytC2 and SyrB1) was effected by treatment with Sfp, a phosphopantheinyl transferase from *Bacillus subtilis* (*30*), according to the following procedure (*17*, *29*). The apo form of the carrier protein (300 μM) was incubated with 10 μM Sfp, 50 mM $MgCl_2$, and 1.5 mM PPant precursor, coenzyme A, at room temperature for 1.5 h with occasional stirring (100−200 mL). The mixture was concentrated and loaded onto a Sephadex G-75 gel filtration column [26 mm (inner diameter) × 100 cm] equilibrated with 20 mM Na-HEPES (pH 7.5). Fractions containing phosphopanthetheinylated carrier protein were pooled, concentrated, and flash-frozen.

The PPant cofactor of SyrB1 (at a final concentration of 1−5 mM) was charged with an amino acid by incubation with 10 mM ATP, 10 mM $MgCl_2$, and 10 mM amino acid at room temperature. To append the amino acid to holo-CytC2 (at a final concentration of 10−25 mM), the reaction mixture was supplemented with catalytic amounts of CytC1 (∼10-fold less than holo-CytC2). The reaction mixture was prepared, and O_2 was removed as previously described (*11*) for subsequent stopped-flow absorption or rapid freeze-quench Mössbauer experiments. The efficiency of PPant attachment and subsequent charging of the PPant by the amino acid was determined by titration of the free thiol content of SyrB1 and CytC2 with Ellman's reagent (DTNB). The ΔA_{412} signal (ε = 13600 M^{-1} cm^{-1}) from the free thiols in the carrier proteins (one Cys residue in SyrB1 and none in CytC2) is first enhanced by attachment of the PPant (giving two total thiols in SyrB1 and one in CytC2) and subsequently diminished due to protection by the amino acid during the charging reaction. The change in the intensity of the signal was used to calculate the extent of PPant attachment and amino acid charging. Treatment of an ATP-depleted reaction mixture with the thioesterase, TycF (*32*), at room temperature after charging by the amino acid resulted in a complete regain of the absorbance that was lost during the charging step, confirming the specificity of the Ellman's signal.

Stopped-Flow Absorption Experiments and Kinetic Analysis. In an anaerobic glovebox (MBraun, Stratham, NH), buffered [20 mM HEPES (pH 7.5)], O_2-free stock solutions of sodium chloride, αKG, and ferrous ammonium sulfate were added to a concentrated, O_2-free [accomplished as previously described (*11*)] solution of apo-SyrB2 at 5 °C to final concentrations of 100 mM, 10 mM, 300 μM, and 360 μM, respectively. Subsequently, deoxygenated substrate (at 5 °C) was added to give at least a 3-fold excess of substrate over Fe(II) (except in the experiments to vary this ratio explicitly). The resultant SyrB2·Fe(II)·αKG·Cl^-· substrate complex was mixed with an equal volume of oxygen-saturated buffer (∼1.8 mM O_2) at 5 °C in an Applied Photophysics (Surrey, U.K.) SX.18MV stopped-flow apparatus with a monochromatic light source and photomultiplier detector, as previously described (*11*). The absorbance at 318 nm, diagnostic of the Fe(IV) intermediate in the Fe(II)- and αKG-dependent hydroxylases (TauD and P4H) and halogenases (CytC3), was monitored with time. The A_{318} versus time traces were fit (using Kaleidagraph from Synergy Software, Reading, PA) by eq 1 describing the absorbance from species I in an R → I → P reaction sequence in which R and P do not absorb. In this equation, k_1 and k_2 are the rate constants for formation and decay of the

intermediate, respectively, $[R]_o$ is the initial concentration of the reactant, R, and ε_I is the molar absorptivity of the intermediate species, I.

$$A_t = [R]_o \varepsilon_I [k_1/(k_2 - k_1)](e^{-k_1 t} - e^{-k_2 t}) \quad (1)$$

Preparation of Freeze-Quenched Mössbauer Samples. Preparation of freeze-quenched samples was as previously described (*33*). A reactant solution containing all components but O_2 was mixed with O_2-saturated buffer, and the reaction mixture was rapidly frozen after the desired reaction time. Reactant solutions used with the L-Thr-, L-Val-, and d_8-L-Val-containing substrates were prepared essentially as described above for the stopped-flow experiments, with the exception that natural abundance Fe(II) was replaced with ^{57}Fe(II). After the solution had been mixed, the composition of samples prepared with the L-Thr substrates was as follows: 610 μM ^{57}Fe, 700 μM SyrB2, 776 μM substrate, 3.3 mM αKG, and 10 mM NaCl; the composition of samples prepared with L-Val and d_8-L-Val substrates was as follows: 406 μM ^{57}Fe, 430 μM SyrB2, 1.28 mM substrate, 5 mM αKG, and 25 mM NaCl.

Preparation of Manually Frozen Mössbauer Samples by Direct Oxygenation with $O_2(g)$. O_2-free solutions of SyrB2, αKG, NaCl, ^{57}Fe(II), and L-Ala- or L-Cpg-containing substrate were combined to give concentrations of 1.2, 5, 50, 1.2, and ≥3 mM, respectively. The solution was placed in a sealed vacuum flask that was stirred vigorously on ice by a magnetic stir bar thick enough to project above the surface of the solution. The flask was briefly evacuated to < 50 Torr and then refilled with 2 atm of O_2(g). After the contents had been vigorously stirred for an additional 1 min at 0 °C, the flask was opened to air and incubation on ice without stirring was continued. Samples were removed at appropriate reaction times and added to Mössbauer sample cups that were then frozen and stored in liquid N_2.

Mössbauer Spectroscopy and Analysis. Mössbauer spectra were recorded on a spectrometer from WEB research (Edina, MN) equipped with a SVT-400 cryostat (Janis, Wilmington, MA) with the temperature of the sample maintained at 4.2 K. The reported values of the isomer shift are relative to the centroid of a metallic foil of α-Fe at room temperature. Analysis of the Mössbauer spectra was carried out using WMOSS from WEB research. The concentration of the Fe(IV) species in each sample was determined as the product of the fractional contribution of its "reference" spectrum to each experimental spectrum and the total ^{57}Fe concentration. Reference spectra for the Fe(IV) states with the different substrates were generated from the experimental spectra of samples with the maximum concentration of the intermediate by removing the features of the other components present in the samples. These include the high-spin Fe(II) reactant and product complexes, which generally exhibit distinguishable quadrupole doublet features (*12*, *23*, *34*). Analyses of 4.2 K/zero-field spectra over a range of Doppler velocities of approximately ±4 mm/s were used to determine the parameters and fractional contributions of the Fe(IV) and Fe(II) complexes. In addition, spectra collected on samples with d_8-L-Val-*S*-SyrB1, L-Ala-*S*-SyrB1, or L-Cpg-*S*-SyrB1 as substrate, in particular, samples frozen after prolonged reaction times, were found to contain significant quantities of the broad and magnetically split features typical of mononuclear high-spin Fe(III), which is often observed as a consequence of univalent decay of the Fe(IV) intermediate(s). For samples containing high-spin Fe(III) species, 4.2 K/53 mT spectra collected over a wider range of Doppler velocities (approximately ±12 mm/s) were used to determine the relative amounts of the components. The spectrum of a sample of the SyrB2·Fe(II)·αKG·Cl^-·HS-SyrB1 complex after reaction with O_2 for 17 min (Figure S2 of the Supporting Information) is dominated by similar Fe(III)-associated features and was used to remove these features from the spectra of samples with d_8-L-Val-*S*-SyrB1, L-Ala-*S*-SyrB1, and L-Cpg-*S*-SyrB1 substrates prior to further spectral analysis.

Experimental reference spectra for the Fe(IV) complexes were generated by removing the experimental reference spectra of the other components as previously described (*12*, *23*, *34*). In addition, spectra were fit by multiple quadrupole doublets, representing the two Fe(IV) complexes of the chloroferryl state and the high-spin Fe(II) complexes. The sum of the two Fe(IV)-associated doublets was used as a theoretical reference spectrum for the chloroferryl state. An alternative experimental reference spectrum for the chloroferryl state was obtained by subtraction of the theoretical contribution of the Fe(II) complexes from the raw spectrum by using its best-fit quadrupole doublet. The different methods of generating reference spectra of the Fe(IV) intermediates yielded nearly identical parameters (approximately ±0.03 mm/s) and fractional contributions (approximately ±5%) (see Table S1 of the Supporting Information).

Preparation of Samples for X-ray Absorption Spectroscopy (XAS). Samples of the intermediate formed in the presence of the L-Cpg-*S*-CytC2 substrate were prepared as described above by direct oxygenation at 0 °C (see above), placed in Mössbauer and XAS sample cups (*35*), and rapidly frozen by immersion in isopentane (total reaction time of ∼4 min). The final concentrations were 1.98 mM ^{57}Fe, 2.47 mM SyrB2, 5 mM αKG, 50 mM NaCl, and 5.9 mM L-Cpg-*S*-CytC2. Samples of the reactant complex not exposed to O_2 were also prepared.

XAS Data Collection and Analysis. XAS data were collected in fluorescence mode at ∼10 K with a 30-element germanium detector (SSRL, BL7-3) using a Si(220) Φ = 90° double-crystal monochromator with a 9.5 keV cutoff for harmonic rejection. To minimize the effects of photoreduction, samples were moved in the beam so that unexposed sample was examined every two scans (exposure time at each spot of ∼30 min, ∼15 min per scan). The edge energy did not shift during the two scans (Figure S3 of the Supporting Information), demonstrating that photoreduction was not a problem. XAS data were obtained by averaging 11 total first and second scans for each state. Background removal and analysis of the EXAFS data were accomplished with EXAFSPAK (available at http://www.ssrl.slac.stanford.edu/exafspak.html). Fits were also obtained by using EXAFSPAK and ab initio phases and amplitudes generated with FEFF version 7.0 (*36*). Data sets were fit over the region k = 3−13 Å^{-1} (for samples of the intermediate) and k = 2−12 Å^{-1} (for samples of the reactant complex). Both complexes were fit with coordination numbers, N, ranging from 3 to 7. Coordination numbers were constrained during fits. All distances, R, and Debye−Waller factors, σ^2, were treated as adjustable parameters, and all threshold energy shifts, E_0, were linked but allowed to vary. The passive electron reduction factor, S_0, was held at 0.9. Edge energies were calibrated using α-Fe metal foil (7111.3 eV). Edge positions were obtained from the first derivative of the data using EXAFSPAK (1.0 eV smoothing, third-order polynomial).

Density Functional Theory Calculations. Calculations were performed with Gaussian 03 using the B3LYP functional. Geometry optimizations were performed with the 6-311G basis

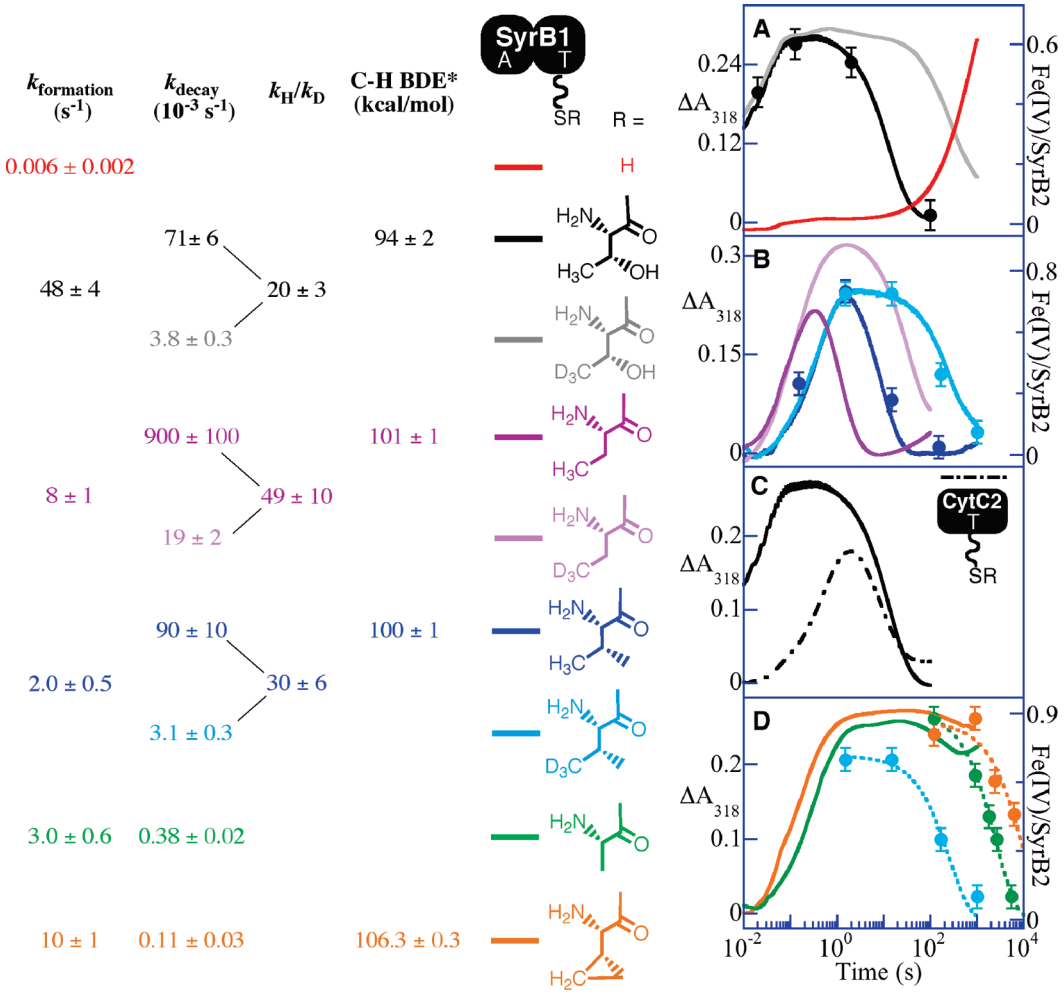

FIGURE 1: Absorbance (318 nm) versus time traces obtained after O_2-saturated buffer [20 mM HEPES (pH 7.5)] was mixed at 5 °C with an equal volume of an O_2-free solution containing SyrB2 (360 μM), Fe(II) (300 μM), αKG (10 mM), and Cl^- (100 mM) in the absence of substrate (A, red trace) or in the presence of the indicated substrate (≥750 μM). Substrates include forms of SyrB1 (solid lines) or CytC2 (dotted−dashed lines) charged with L-Thr (A and C, black trace), d_5-L-Thr (A, gray trace), L-Ala (D, green trace), L-Aba (B, dark pink trace), d_6-L-Aba (B, light pink trace), L-Val (B, dark blue trace), d_8-L-Val (B, light blue trace), and L-Cpg (D, orange trace). Filled circles indicate the equivalents of total Fe(IV) determined by Mössbauer spectroscopy. For the d_8-L-Val, L-Cpg, and L-Ala substrates in panel D, the data points obtained from the Mössbauer experiments were fit by the equation for an exponential decay (light blue, green, and orange dashed decay traces) to obtain the values of k_{obs} for decay quoted in the text. *The BDEs indicated in the scheme (*44*) correspond to the target C−H bond strengths of small molecules representative of the amino acid side chain: 2-propanol, propane, isobutane, and cyclopropane correspond to the side chains of L-Thr, L-Aba, L-Val, and L-Cpg, respectively.

set (*37*). The coordinates from the crystal structure (Protein Data Bank entry 2FCT) (*22*) were used to create the starting model for the Fe(II) reactant complex. Only metal ligands were retained. Histidine was truncated to imidazole and αKG to pyruvate. The starting model for geometry optimizations of the chloroferryl state was obtained from the reactant complex. The water ligand was replaced with an oxygen atom and the pyruvate with acetate.

RESULTS AND DISCUSSION

Substrate Triggering (ST) in SyrB2. (i) Testing for Chloroferryl Intermediate Accumulation and ST in SyrB2. To test for ST in SyrB2, its reaction with O_2 in the presence of the complete, native substrate, SyrB1 charged by L-Thr (L-Thr-*S*-SyrB1) (*17*), was first examined. When an anoxic solution containing SyrB2, Fe(II), αKG, Cl^-, and L-Thr-*S*-SyrB1 is mixed at 5 °C with O_2-saturated buffer, the absorbance at 318 nm (A_{318}) increases to a maximum with an apparent first-order rate constant, k_{obs}, of 48 ± 4 s^{-1} (with O_2 in excess at ~0.9 mM) and then decays to its initial value with a k_{obs} of (71 ± 6) × 10^{-3} s^{-1} (Figure 1A, black trace). Analogy to previous results for TauD, P4H, and CytC3 would suggest that the A_{318} transient reflects accumulation and decay of the hydrogen-abstracting chloroferryl intermediate state. This inference is confirmed by the ^2H KIE of ~20 on the decay phase (Figure 1A, gray trace) seen upon use of L-Thr-*S*-SyrB1 having all five exchange-inert hydrogen atoms of the L-Thr (including those in the target side chain methyl group) substituted with deuterium (d_5-L-Thr). More directly, the 4.2 K/zero-field Mössbauer spectra of freeze-quenched samples from the reaction (Figure 2A) exhibit transient features that can be analyzed as a pair of partially resolved quadrupole doublets with the following parameters: δ_1 = 0.30 mm/s and ΔE_{Q1} = 1.09 mm/s (red line in Figure 2A) and δ_2 = 0.23 mm/s and ΔE_{Q2} = 0.76 mm/s (blue line). The similarity of these parameters to those determined previously for the chloroferryl state in CytC3 (*23*) confirms the accumulation of the corresponding state in the SyrB2 reaction. The presence of two doublets at an intensity ratio that is essentially constant with time (at ~4:1) suggests that, as in the CytC3 reaction, the SyrB2 intermediate state comprises two Fe(IV) complexes in equilibrium. Although

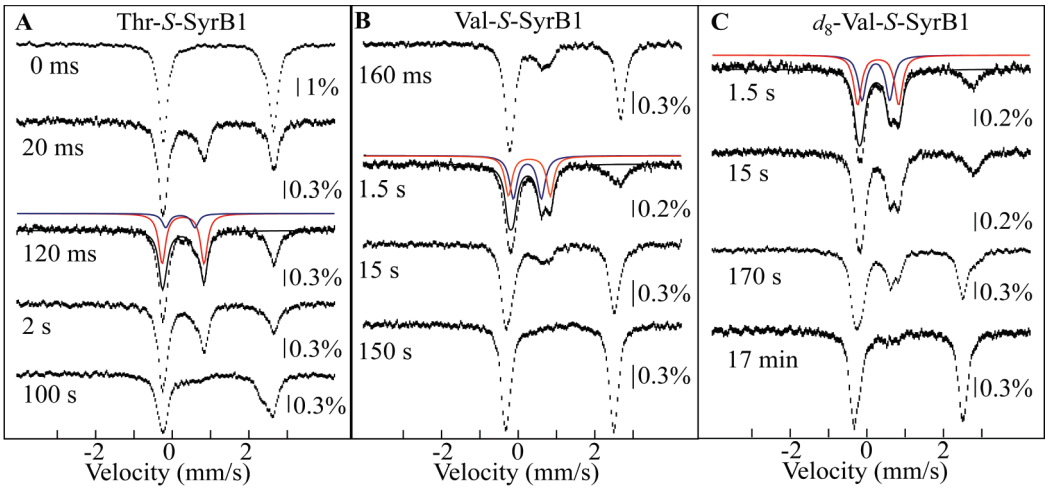

FIGURE 2: Mössbauer spectra (4.2 K/0 mT) of selected samples prepared by reacting the SyrB2·Fe(II)·Cl^-·αKG·substrate complex at 5 °C with O_2-saturated buffer. Substrates and reaction times are indicated. The final sample compositions are given in Materials and Methods. Solid lines are simulations of the spectra of the two Fe(IV) components of the chloroferryl state (red and blue) and the summation of their contributions (black). The isomer shift and quadrupole splitting parameters of the Fe(IV) intermediate(s) are as follows: for L-Thr, $\delta_1 = 0.30$ mm/s, $\Delta E_{Q1} = 1.09$ mm/s, $\delta_2 = 0.23$ mm/s, and $\Delta E_{Q2} = 0.76$ mm/s; for L-Val and d_8-L-Val, $\delta_1 = 0.29$ mm/s, $\Delta E_{Q1} = 1.09$ mm/s, $\delta_2 = 0.24$ mm/s, and $\Delta E_{Q2} = 0.73$ mm/s.

the ~4:1 intensity ratio in SyrB2 is different from the ~1:1 ratio seen in CytC3, results presented below show that the SyrB2 ratio varies with the amino acid that is tethered to SyrB1. From the sum of the contributions of the two Fe(IV)-associated doublets to the total absorption area of each Mössbauer spectrum, the kinetics of the SyrB2 intermediate state were determined (black circles in Figure 1A). They coincide well with the ΔA_{318} versus time traces.

Replacement of L-Thr-*S*-SyrB1 with SyrB1 lacking an amino acid on its PPant cofactor (HS-SyrB1) markedly changes the reaction kinetics (Figure 1A, red trace). UV absorption develops 8000-fold less rapidly and is stable rather than transient (on the 1000 s maximum time scale of the stopped-flow apparatus). Moreover, the slowly developing absorption is not associated with the chloroferryl intermediate state, as the 4.2 K/zero-field Mössbauer spectrum of a sample freeze-quenched at approximately the half-time of the rise phase lacks the signature of the intermediate (spectrum A in Figure S1 of the Supporting Information). At completion of the rise phase, features characteristic of high-spin Fe(III) species dominate the Mössbauer spectrum (Figure S2 of the Supporting Information). Reactions entirely without SyrB1 or with SyrB1 lacking its PPant cofactor give ΔA_{318} versus time traces nearly identical to that for the reaction with HS-SyrB1 (not shown). Inclusion in the reaction mixture of free L-Thr or its carboxylate → alcohol analogue, L-threoninol (chosen with the intent of mimicking the charge-neutralizing effect of thioesterification of L-Thr with the PPant thiol), together with HS-SyrB1 does not noticeably accelerate the reaction. In short, the complete, native substrate, L-Thr-*S*-SyrB1, triggers reaction of SyrB2 with O_2 by 8000-fold and may even change the reaction mechanism [in light of the fact that (i) the chloroferryl state does not accumulate and (ii) Fe(III) rather than Fe(II) products are generated in the "untriggered" reaction]; the tethered amino acid is necessary for ST, and neither the free amino acid nor a carboxylate-neutralized analogue of it has any triggering effect. The incompetence of free amino acids for ST may be partly (if not completely) responsible for their reported failure to be halogenated (*20*, *21*, *38*, *39*). The factor by which SyrB2 is triggered by its native substrate is greater than any yet observed for a member of this enzyme family. By comparison, TauD is triggered by 1000-fold (*25*, *26*), PBCV-1 P4H by 500-fold (*12*), and CytC3 by 40-fold under similar reaction conditions.

(ii) Dependence of ST Efficacy on the Structure of the Amino Acid Side Chain. Having established that ST is operant in SyrB2 and that the tethered amino acid is essential for it, we next addressed whether the structure of the amino acid, or merely the fact that it caps the PPant as a thioester, is more important for ST. SyrB1 species representing (i) replacement of the hydroxyl group of the L-Thr side chain with either hydrogen (L-Aba-*S*-SyrB1, where L-Aba denotes L-2-aminobutyric acid) or a second methyl (L-Val-*S*-SyrB1), (ii) replacement of the target methyl with hydrogen (L-Ser-*S*-SyrB1), and (iii) replacement of both β-substituents with hydrogens (L-Ala-*S*-SyrB1) were tested for ST efficacy under the same reaction conditions used for the native substrate. Qualitatively, each of the four non-native amino acids triggers the O_2 reaction when tethered to SyrB1 (Figure 1B,D). In every case, UV absorption develops with a k_{obs} of 2−8 s^{-1}, more than 2 orders of magnitude faster than the reaction with HS-SyrB1. For the two substrates retaining the γ-methyl halogenation target (L-Aba-*S*-SyrB1 and L-Val-*S*-SyrB1), the attribution of the transient absorption to the chloroferryl intermediate state is confirmed by two lines of evidence. For both substrates, large ^2H KIEs on the decay phases (Figure 1B, compare light and dark traces) demonstrate that the intermediate abstracts hydrogen. For L-Val-*S*-SyrB1, Mössbauer spectra of freeze-quench samples (Figure 2B,C, yielding blue circles in Figure 1B) from the reactions of both unlabeled and deuterium-labeled substrates demonstrate both accumulation of the chloroferryl state and the coincidence of its kinetics with the A_{318} transients. For the substrates lacking the γ-methyl halogenation target (L-Ala-*S*-SyrB1 and L-Ser-*S*-SyrB1), the UV absorption fails to decay on the maximum time scale (1000 s) of the stopped-flow apparatus (Figure 1D, green trace). This observation is consistent with the expectation that the absence of the target hydrogen should stabilize the chloroferryl state to an even greater extent than deuterium substitution, as is verified and discussed in more detail in a later section.

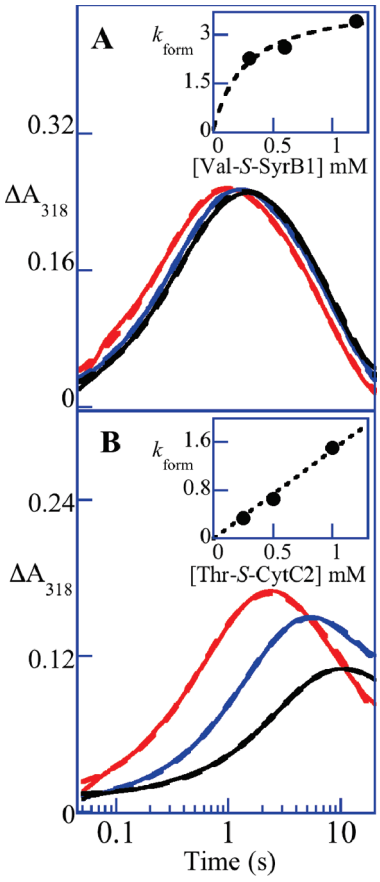

FIGURE 3: Dependencies of ST efficacy on the concentrations of two non-native substrates in the reactions of the Fe(II)·SyrB2·αKG·Cl^-·substrate complex with O_2 at 5 °C. A_{318} versus time traces from stopped-flow experiments in which the concentration of L-Val-*S*-SyrB1 (A) or L-Thr-*S*-CytC2 (B) was varied from 0.30 mM [2-fold excess over the SyrB2·Fe(II)·αKG·Cl^- complex (black trace)] to 0.60 mM [4-fold excess (blue trace)] to 1.2 mM [8-fold excess (red trace)]. The insets show plots of the k_{obs} for formation (in units of s^{-1}) from regression analysis as a function of substrate concentration. In panel A, the data points (●) are fit best by a hyperbola characteristic of saturation of SyrB2 by L-Val-*S*-SyrB1. By contrast, the inset of panel B shows a linear dependence of the k_{obs} for formation on L-Thr-*S*-CytC2 concentration, indicative of weak binding of the substrate to SyrB2.

Quantitatively, the triggering efficacies (as assessed by k_{obs} for chloroferryl intermediate formation under a common set of reaction conditions) of the four non-native substrates are 5−24-fold less than that of the native substrate. In principle, the diminished efficacy could reflect diminished binding affinity for the non-native substrate or less profound activation of the Fe(II) cofactor toward reaction with O_2 in the complex (or a combination of the two). To address this issue, variation of the concentration of one of the non-native substrates (L-Val-*S*-SyrB1) was carried out. The value of k_{obs} for the formation phase extracted by regression analysis of the traces in Figure 3A increases by less than 50% as the concentration of L-Val-*S*-SyrB1 is increased by a factor of 4 (inset). This kinetic order of much less than one implies saturation of SyrB2 by the non-native substrate at the higher ratios. If the dependence of k_{obs} on L-Val-*S*-SyrB1 concentration is treated as a hyperbolic function, the limiting *y* value (3.7 s^{-1}) is less than one tenth of the k_{obs} for the native substrate reaction at a L-Thr-*S*-SyrB1:SyrB2 ratio of 3 (which is saturating). This analysis implies that the identity of the amino acid affects the O_2 reactivity of the complex, in addition to any effect on affinity that it may have. The observations suggest that the halogenase makes important contacts both with the PPant-thioester terminus and with both substituents on the β-methine carbon of the appended L-Thr, as any modification of the side chain diminishes ST efficacy without eliminating the considerable (≥400-fold) activation conferred by the attachment of any amino acid. It is possible that even further truncation of the native L-Thr (e.g., Gly or perhaps even acetyl) might be tolerated without loss of this side chain-independent contribution to ST. We attempted to test Gly but found that the adenylation module of SyrB1 was unable to charge the side chain-less amino acid onto the PPant of the carrier domain.

(iii) Dependence of ST Efficacy on the Identity of the Carrier Protein. Having established (i) that ST is operant in SyrB2, (ii) that attachment of any amino acid to the PPant of SyrB1 is quantitatively most important for it, and (iii) that its efficacy is still moderately sensitive to the structure of the amino acid side chain, we next asked whether the structure of the carrier domain has an impact on ST efficacy. L-Thr was appended to CytC2, the carrier protein for the CytC3 halogenase from the cytotrienin biosynthetic system (Scheme 2B) (*29*). Whereas SyrB1 comprises an adenylation (A) domain to activate the amino acid for attachment to the PPant on its thiolation (T) domain (Scheme 2A), CytC2 is a stand-alone thiolation domain (which is charged with the amino acid by the separate adenylation protein, CytC1) and is consequently smaller (11.5 kDa, including the affinity tag) than SyrB1 (66 kDa), a characteristic potentially useful for accumulation of the intermediate state to very high concentrations (see below). L-Thr-*S*-CytC2 triggers formation of the chloroferryl intermediate state in SyrB2 (Figure 1C). Quantitatively, it is less effective than the native substrate by ~40-fold at the same concentration. However, the linear dependence on L-Thr-*S*-CytC2 concentration of k_{obs} for the development phase of the A_{318} transient (Figure 3B) suggests that the diminished ST efficacy of the substrate containing the native amino acid tethered to the heterologous carrier protein could reflect primarily a diminished affinity for the halogenase. Together, the data suggest that the carrier protein provides the more important binding determinants for complex formation, delivering the amino acid to the halogenase active site, and that specific contacts with the side chain then condition the active site in a manner that further activates for O_2 addition and chloroferryl intermediate formation.

Effects of the Side Chain on the Chloroferryl State and its C−H Bond Cleavage Efficiency. The amino acid side chain exerts three additional, intriguing effects on the halogenase reaction. The first is on the distribution of the intermediate state between its two constituent complexes, as reflected by the relative contributions of the two partially resolved Mössbauer quadrupole doublets. Whereas the ratio is ~4:1 with the native substrate (Figure 2A), it is ~1:1 with L-Val-*S*-SyrB1 (Figure 2B). With the L-cyclopropylglycine substrate (L-Cpg-*S*-SyrB1) discussed in the next section, the ratio shifts even further to ~1:5. The ability to change the composition of the intermediate state potentially provides a tool for understanding the structural distinction between its constituent complexes. It also contrasts with previous observations on CytC3, in which the chloroferryl state was shown to have a ~1:1 ratio of the two putative coordination isomers when formed with either L-Aba- or L-Val-charged CytC2 (*23*). The second effect is on the electronic structure of the iron in the chloroferryl state, as reflected by the Mössbauer parameters. In particular, the quadrupole splitting

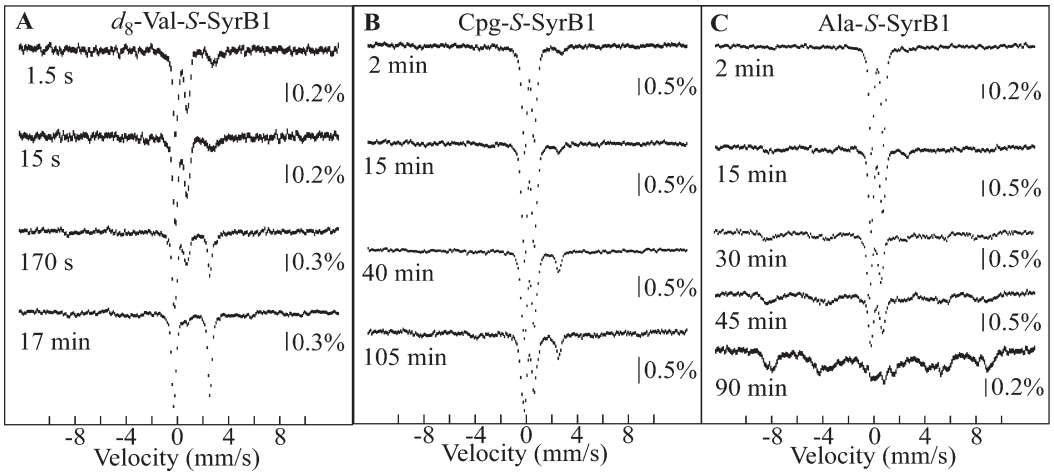

FIGURE 4: Mössbauer spectra (4.2 K/53 mT) of selected samples collected over an approximately ±12 mm/s range of Doppler velocities to obtain the decay kinetics of the chloroferryl state formed by reacting the SyrB2·Fe(II)·Cl^-·αKG·substrate complex at 5 °C with O_2. Substrates and reaction times are indicated. The final compositions of the samples are given in Materials and Methods.

parameter (ΔE_Q) of chloroferryl species 1 prepared with substrates having two non-hydrogen substituents at C_β (i.e., L-Thr-*S*-SyrB1, L-Val-*S*-SyrB1, and L-Cpg-*S*-SyrB1) is larger than that for the complex prepared with substrates having only one (L-Aba-*S*-SyrB1) or no C_β substituent (L-Ala-*S*-SyrB1) (1.09−1.14 mm/s compared to 0.99 mm/s). The third effect is on the kinetics of decay of the chloroferryl state. The A_{318} kinetic traces for the L-Val-*S*-SyrB1 and L-Aba-*S*-SyrB1 reactions (Figure 1B) show that decay of the chloroferryl state to the Fe(II) product state by C−H bond cleavage and (presumably) chlorination is at least 10-fold faster for the substrate lacking the second γ-methyl group, despite the fact that the target C−H bonds are expected to have similar homolytic bond dissociation energies (BDEs; listed on the left of Figure 1). Conversely, the rate constants for decay with the β-disubstituted L-Val- and L-Thr-containing substrates are nearly identical (compare panels A and B of Figure 1), despite the expectation that their C−H BDEs should differ considerably. In addition, the [^{2}H]KIE is somewhat greater for the faster reaction (∼50 for L-Aba-*S*-SyrB1) than for the two slower reactions (∼20 for L-Thr-*S*-SyrB1 and ∼30 for L-Val-*S*-SyrB1). The origins of these kinetic effects are not clear, but it is possible that the absence of the second substituent on C_β (hydroxyl or methyl) to anchor the side chain within the SyrB2 active site allows the target hydrogen to achieve greater proximity or more frequent close approach to the chloroferryl oxygen, a situation expected to favor both more rapid C−H cleavage and a larger [^{2}H]KIE (*40*).

Exploring the Limit of Stability of the Chloroferryl Intermediate in SyrB2. (i) Unprecedented Protection of the Chloroferryl State by SyrB2. Figures 1B and 2C illustrate that the chloroferryl intermediate in SyrB2 decays remarkably slowly [$k = (3.1 \pm 0.3) \times 10^{-3}$ s^{-1}] in its reaction with the deuterium-labeled L-Val-*S*-SyrB1 substrate. Indeed, the half-life of almost 3 min (at 5 °C) is the longest yet observed for a non-heme ferryl enzyme intermediate (*4*, *11*−*13*, *23*, *41*).[2] Moreover, the spectra in Figure 3A illustrate that, despite its long lifetime, the intermediate decays primarily (>70%) to Fe(II) products, which occurs in productive halogenation (which was not explicitly demonstrated). This observation contrasts with previous results on CytC3, in which decay of the intermediate in the presence of the deuterium-labeled substrate, 4,4,4-d_3-L-Aba-*S*-CytC2, was seen to yield more Fe(III) complex(es), suggesting that unproductive univalent reduction of the intermediate competes effectively with the productive pathway initiated by deuterium abstraction (*23*). The implication is that SyrB2 suppresses the alternative decay pathway(s) to a greater extent than does CytC3. This suppression is also much greater than for TauD, the only other member of the family for which data are available to assess this issue (*26*). Evidence suggests that, in TauD, a specific tyrosine residue (Y73) near the Fe cofactor can be oxidized to a radical, providing a potential source of the electron for univalent decay of the ferryl complex (*43*). SyrB2 possesses multiple tyrosine residues in similar proximity to its cofactor. Why these Y residues do not reduce the chloroferryl state more efficiently (i.e., how SyrB2 prevents this undesired side reaction) is an intriguing question for future investigation.

(ii) Extending the Lifetime of the Chloroferryl State by Target Removal or Modification. The unusually effective suppression of alternative, unproductive pathways for decay of the chlorinating intermediate, combined with the modularity of the SyrB2 substrate and tolerance for significant side chain modifications, suggested the opportunity for further stabilization of the intermediate. To explore the limit of stabilization of the chloroferryl complex by SyrB2, we tested two alternative substrates, the aforementioned L-Ala-*S*-SyrB1 and L-Cpg-*S*-SyrB1. The former substrate lacks the chlorination target altogether, and the latter possesses a stronger target C−H bond [BDE of ∼106 kcal/mol (*44*)] that we anticipated might be too strong for the chloroferryl intermediate to cleave (see Figure 1). In each reaction, A_{318} develops with kinetics (Figure 1D, solid traces) similar to those observed for the L-Val substrate (Figure 1B, dark blue trace). Consistent with the desired stabilization of the intermediate (and as noted above for the L-Ala-*S*-SyrB1 reaction), A_{318} does not decay in the 1000 s upper time limit of the stopped-flow apparatus. This stability allows the intermediate to be prepared in high yield by exposure of a solution of the SyrB2·substrates complex to O_2(g) rather than by the more common procedure of rapid mixing with O_2-saturated

[2]Even longer-lived non-heme ferryl species have been documented in inorganic coordination chemistry. Que and co-workers reported ferryl complexes with half-lives of 6 and 60 h at 25 °C. Analogous to the SyrB2 chloroferryl state, these inorganic ferryl complexes are, despite their remarkakable stability, sufficiently potent oxidants to cleave strong C−H bonds, including the ∼99 kcal/mol C−H bond of cyclohexane (*42*).

buffer (see Materials and Methods for the procedure and below for its technical advantages). Mössbauer spectra of samples prepared in this manner confirm accumulation of the Fe(IV) state in both reactions (Figure 4B,C). For the L-Cpg-*S*-SyrB1 reaction, the Fe(IV)-associated Mössbauer features can be analyzed as two doublets with an ~1:5 intensity ratio (Figure S1, spectrum F) and essentially the same parameters (δ_1 = 0.32 mm/s, ΔE_{Q1} = 1.12 mm/s, δ_2 = 0.25 mm/s, and ΔE_{Q2} = 0.69 mm/s) observed for the intermediate formed with the L-Thr- and L-Val-appended substrates. Immediately after the direct oxygenation procedure, the intermediate state constitutes 88 ± 5% of the ^{57}Fe, giving a concentration of >1 mM. The spectra of samples frozen at various times during the subsequent incubation of the solution in air at 0 °C imply that the state decays very slowly ($t_{1/2}$ ~ 1.8 h). With the L-Ala-*S*-SyrB1 substrate, the intermediate accumulates to similarly high levels (90 ± 5%). In this case, the Mössbauer features can be satisfactorily ascribed to a single quadrupole doublet with a δ of 0.27 mm/s and a ΔE_Q of 0.94 mm/s (not shown), but the asymmetry of the high-energy line and increased width of both lines (~0.30 mm/s) suggest that two complexes might still be present. If so, their parameters are perturbed relative to the aforementioned cases, resulting in diminished spectral resolution (Figure S1, spectrum E; Table S1). Upon subsequent prolonged incubation, the quadrupole doublet features of the intermediate decay with a $t_{1/2}$ of 30 min. In the reactions of both substrates, features characteristic of high-spin Fe(III), rather than the high-spin Fe(II) generated upon productive halogenation, grow in as the intermediate decays (Figure 4B,C). Thus, with the methyl chlorination target removed or modified to strengthen the C−H bond, the chloroferryl state decays by univalent reduction. The fact that the intermediate is less stable when it is formed with L-Ala-*S*-SyrB1 than when it is formed with L-Cpg-*S*-SyrB1 suggests that packing of the side chain in the active site may be important not only for optimal ST but also for optimal protection of the high-valent complex(es) against unproductive decay pathways.

Characterization of the Stabilized Chloroferryl Intermediate by EXAFS Spectroscopy. The unprecedented stability of the SyrB2 chloroferryl state[2] effectively removes several challenges inherent to the use of the rapid-mix/freeze-quench method to prepare such intermediates for structural characterization (e.g., concentration limits imposed by the limited solubility of O_2, diminished accumulation caused by competition from the decay process, dilution of the intermediate by mixing the freeze-quench cryo-solvent, and poor transmittance of the packed-powder samples produced by the method). It thereby potentially permits application of biophysical methods requiring a higher concentration or purity (e.g., nuclear resonance vibrational spectroscopy), optical-quality samples (e.g., magnetic circular dichroism spectroscopy), or extreme stability (e.g., X-ray crystallography). EXAFS spectroscopy is one such high-resolution structural technique that benefits from samples with a high concentration and, more importantly, purity. Although EXAFS spectroscopy was previously applied to the bromoferryl state of the CytC3 halogenase to determine Fe−oxo and Fe−Br distances (*24*), neither the presence of the Cl−Fe=O unit nor either bond distance has been established for the more relevant chloroferryl state. To begin to capitalize on the virtues of the SyrB2 system revealed above, we prepared the chloroferryl intermediate state at a high concentration and purity for characterization by EXAFS. The smaller CytC2 carrier protein was used for ST, the L-Cpg amino acid was appended for maximum

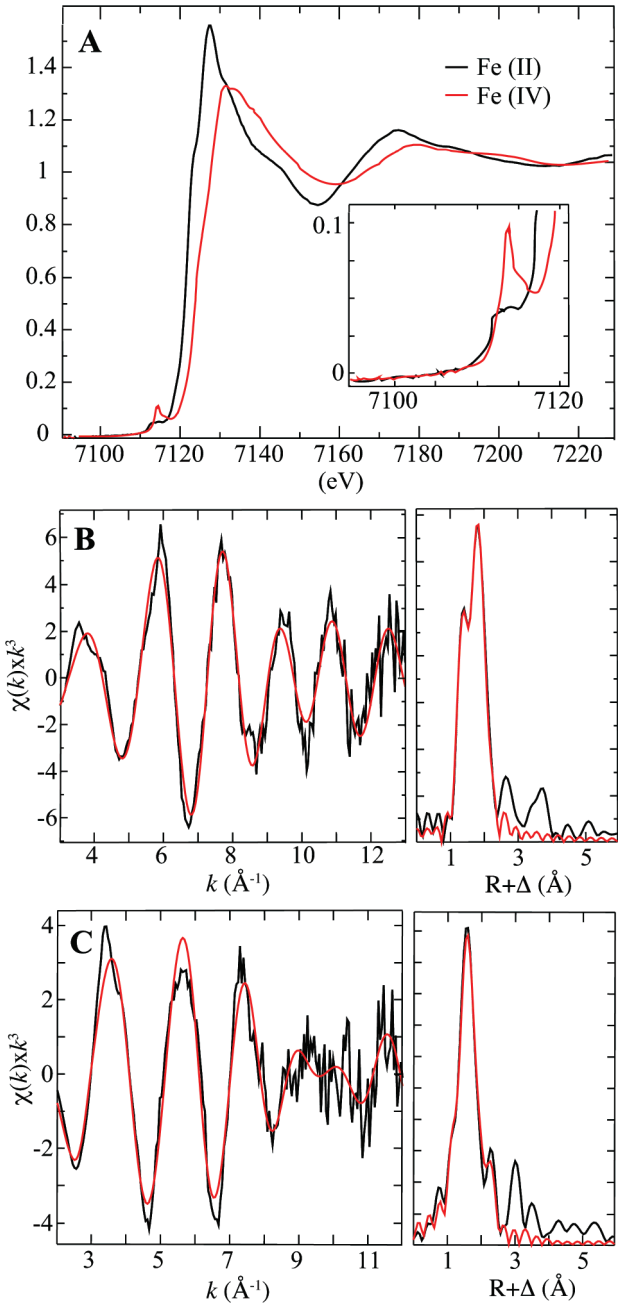

FIGURE 5: Fe K-edge X-ray absorption data for the SyrB2·Fe(II)·αKG·Cl$^-$·L-Cpg-*S*-CytC2 sample (A, black trace) and samples enriched in the chloroferryl state by reaction of this complex with O_2 (A, red trace). The pre-edge region is expanded in the inset. EXAFS data for the chloroferryl sample (B, left panel) and Fourier transform of the EXAFS data (B, right panel). The raw data are shown in black, and the best fit is shown in red. The ^{57}Fe Mössbauer spectrum of the same sample is given in the Supporting Information (Figure S1, spectrum G). EXAFS data (C, left panel) for the Fe(II) reactant complex and the Fourier transform of the EXAFS data (C, right panel). The raw data are shown in black, and the best fit is shown in red.

intermediate stability, and the direct oxygenation procedure was used to exceed the concentration limit imposed by O_2 solubility. The Mössbauer spectrum of a parallel sample (Figure S1, spectrum G) demonstrates accumulation of the Fe(IV) state to 90% of the total ^{57}Fe and a concentration of ~1.8 mM.

The K-edge XAS data are shown in Figure 5. The absorption-edge energy for the samples enriched in the chloroferryl state is ~1.9 eV greater than for the samples of the reactant state

Table 1: EXAFS Fitting Results for the SyrB2·Fe(II)·αKG·Cl^-·L-Cpg-*S*-CytC2 Reactant Samples[a]

Fe−O/N			Fe−O or O/N			Fe−Cl				
N	*R*	σ^2	*N*	*R*	σ^2	*N*	*R*	σ^2	E_0	*F*
1	2.18	0.0039	4	2.11	0.0057	1	2.40	0.0029	−5.27	0.349[b]
2	2.21	0.0008	3	2.08	0.0022	1	2.41	0.0037	−4.79	0.347[b]
3	2.17	0.0066	2	2.09	0.0034	1	2.40	0.0035	−4.48	0.348[b]
4	2.12	0.0046	1	1.24	0.0691	1	2.40	0.0023	−4.83	0.359
4	2.14	0.0059	1	2.04	0.0053	1	2.40	0.0032	−5.54	0.350
4	2.12	0.0046	−	−	−	1	2.40	0.0023	−5.11	0.366
5	**2.12**	**0.0064**	−	−	−	**1**	**2.40**	**0.0029**	**−5.20**	**0.349**
6	**2.12**	**0.0083**	−	−	−	**1**	**2.41**	**0.0037**	**−5.15**	**0.349**

[a] Raw data were fit over the $k = 2-12$ Å^{-1} region. The coordination number (*N*), interatomic distance (*R*, in Å), mean square deviation in *R* (Debye−Waller factor, σ^2, in Å^2), and threshold energy shift (E_0, in eV) are shown. *N* was constrained during fits. The best fits are in bold. The fit error, *F*, is defined as $[\sum k^6(\chi_{exptl} - \chi_{calc})^2/\sum k^6\chi_{exptl}^2]^{1/2}$. [b] These fits were excluded as best fits on the basis of the resolution (0.159 Å) of our data.

Table 2: EXAFS Fitting Results for the Samples Enriched in the SyrB2 Chloroferryl Intermediate[a]

Fe−O/N			Fe−O/N			Fe−Cl				
N	*R*	σ^2	*N*	*R*	σ^2	*N*	*R*	σ^2	E_0	*F*
0	−	−	3	2.11	0.0024	1	2.32	0.0010	0.37	0.448
0	−	−	4	2.12	0.0046	1	2.31	0.0019	0.37	0.435
0	−	−	5	2.13	0.0066	1	2.30	0.0025	0.63	0.433
1	1.70	0.0031	3	2.19	0.0007	0	−	−	11.63	0.424
1	1.66	0.0033	3	2.11	0.0021	1	2.32	0.0010	0.37	0.317
1	1.69	0.0032	4	2.18	0.0021	0	−	−	9.40	0.391
1	**1.66**	**0.0038**	**4**	**2.12**	**0.0049**	**1**	**2.31**	**0.0021**	**0.63**	**0.312**
1	1.69	0.0033	5	2.17	0.0032	0	−	−	7.75	0.383
1	**1.67**	**0.0041**	**5**	**2.13**	**0.0073**	**1**	**2.30**	**0.0024**	**0.88**	**0.312**
2	1.68	0.0081	2	2.14	−0.0000	1	2.34	0.0012	6.41	0.362
3	1.60	0.0226	1	2.03	−0.0021	1	2.27	−0.0012	−9.52	0.481

[a] Raw data were fit over the $k = 3-13$ Å^{-1} region. The coordination number (*N*), interatomic distance (*R*, in Å), mean square deviation in *R* (Debye−Waller factor, σ^2, in Å^2), and threshold energy shift (E_0, in eV) are shown. *N* was constrained during fits. The best fits are in bold. The fit error, *F*, is defined as $[\sum k^6(\chi_{exptl} - \chi_{calc})^2/\sum k^6\chi_{exptl}^2]^{1/2}$.

(7122.8 and 7120.9 eV, respectively), demonstrating the greater binding energy of the 1s electron in the Fe(IV) complex(es). The samples of the intermediate also exhibit a (~2.5-fold) more intense pre-edge feature, which arises from the 1s to 3d transition and is commonly observed for ferryl species as a consequence of the axial symmetry imposed by the dominant oxo ligand (*45*, *46*). The data for the reactant state could be fit well by inclusion of two shells of scatterers, one with five O/N ligands at 2.12 Å and the second with a single Cl ligand at 2.40 Å (Table 1). This analysis is consistent with the crystal structure of SyrB2, although the structurally characterized protein did not have the substrate bound. Two other geometries gave slightly diminished fit errors, but they included two shells of O/N ligands at distances too similar to be resolved with the resolution of the data (0.159 Å). The data for the samples of the intermediate state were fit best by inclusion of three shells of scatterers: one short O/N ligand at 1.66 Å (the oxo group), four O/N ligands at 2.12 Å, and one Cl ligand at 2.31 Å. Importantly, the short O/N and Cl scatterers were both required for optimal fits (Table 2). The distances agree well with the geometry-optimized models, which include a Fe−Cl bond of 2.35 Å, a Fe−O bond of 1.64 Å, and an Fe−O/N shell ranging from 1.91 to 2.10 Å. They are also very similar to the bond lengths in the only structurally characterized synthetic chloroferryl complex (*47*). For both SyrB2 redox states, analysis of Fourier-filtered data yielded results essentially identical with those obtained by analysis of the raw data (Tables S1 and S2 of the Supporting Information).

CONCLUSIONS

Substrate triggering, a phenomenon previously shown to occur in several Fe(II)/αKG-dependent oxygenases and thought to protect the enzymes by properly timing the formation of their potently oxidizing ferryl intermediates, is also operant in the structurally and mechanistically related aliphatic halogenase, SyrB2. The complete trimodular substrate, with carrier protein (SyrB1), covalently attached PPant cofactor, and thioester-appended amino acid, is required for ST of rapid chloroferryl intermediate formation. The data suggest that the carrier protein provides the most important binding determinants, delivering the amino acid into the SyrB2 active site, where specific contacts between the halogenase and its substrate's side chain optimally condition its Fe(II) cofactor for O_2 activation [at least in part by promoting dissociation of a weakly bound water ligand (*8*)]. SyrB2 is triggered by its substrate and protects its high-valent intermediate from side reactions to unprecedented extents. The large triggering factor, tolerance for even profound chemical modifications of the side chain, and unprecedented efficiency of containment of the chloroferryl intermediate present opportunities for structural characterization, which we have begun to exploit in this study, measuring Fe−oxo and Fe−Cl distances by EXAFS spectroscopy and showing that these distances are consistent with DFT-derived models. With the abilities to accumulate the intermediate to high concentrations (perhaps > 5 mM), freeze-trap it to obtain ideal sample properties, and stabilize it for hours, application of additional structural techniques, even those with more severe technical demands, may now be undertaken.

SUPPORTING INFORMATION AVAILABLE

Comparison of 4.2 K/zero-field Mössbauer spectra for samples containing maximal amounts of the chloroferryl state formed in the presence of L-Thr-, L-Val-, L-Cpg-, L-Ala-, and d_6-L-Aba-charged SyrB1 substrates; 4.2 K/53 mT Mössbauer spectrum collected over an approximately ±12 mm/s range of Doppler velocities for a sample containing the SyrB2·Fe(II)·αKG·Cl^-·HS-SyrB1 complex that was reacted with O_2 for 17 min; Mössbauer parameters of the two Fe(IV) species formed in the presence of different substrates; overlay of the first- and second-scan XAS K-edge for samples containing the SyrB2··Fe(II)·αKG·Cl^-·L-Cpg-*S*-CytC2 reactant complex and the chloroferryl intermediate state demonstrating that both complexes are resistant to photoreduction; Fourier-filtered EXAFS data for the Fe(II) reactant complex and Fe(IV) intermediate state; coordinates of the optimized geometry of the chloroferryl intermediate; and the complete ref *37*. This material is available free of charge via the Internet at http://pubs.acs.org.

REFERENCES

1. Hausinger, R. P. (2004) Fe(II)/α-ketoglutarate-dependent hydroxylases and related enzymes. *Crit. Rev. Biochem. Mol. Biol. 39*, 21–68.

2. Solomon, E. I., Brunold, T. C., Davis, M. I., Kemsley, J. N., Lee, S.-K., Lehnert, N., Neese, F., Skulan, A. J., Yang, Y.-S., and Zhou, J. (2000) Geometric and electronic structure/function correlations in non-heme iron enzymes. *Chem. Rev. 100*, 235–349.
3. Costas, M., Mehn, M. P., Jensen, M. P., and Que, L.Jr. (2004) Dioxygen activation at mononuclear nonheme iron active sites: Enzymes, models, and intermediates. *Chem. Rev. 104*, 939–986.
4. Krebs, C., Galonić Fujimori, D., Walsh, C. T., and Bollinger, J. M.Jr. (2007) Non-heme Fe(IV)-oxo intermediates. *Acc. Chem. Res. 40*, 484–492.
5. Que, L.Jr. (2000) One motif: Many different reactions. *Nat. Struct. Biol. 7*, 182–184.
6. Koehntop, K. D., Emerson, J. P., and Que, L.Jr. (2005) The 2-His-1-carboxylate facial triad: A versatile platform for dioxygen activation by mononuclear non-heme iron(II) enzymes. *J. Biol. Inorg. Chem. 10*, 87–93.
7. Pavel, E. G., Zhou, J., Busby, R. W., Gunsior, M., Townsend, C. A., and Solomon, E. I. (1998) Circular dichroism and magnetic circular dichroism spectroscopic studies of the non-heme ferrous active site in clavaminate synthase and its interaction with α-ketoglutarate cosubstrate. *J. Am. Chem. Soc. 120*, 743–753.
8. Neidig, M. L., Brown, C. D., Light, K. M., Galonić Fujimori, D., Nolan, E. M., Price, J. C., Barr, E. W., Bollinger, J. M.Jr., Krebs, C., Walsh, C. T., and Solomon, E. I. (2007) CD and MCD of CytC3 and taurine dioxygenase: Role of the facial triad in α-KG-dependent oxygenases. *J. Am. Chem. Soc. 129*, 14224–14231.
9. Hanauske-Abel, H. M., and Popowicz, A. M. (2003) The HAG mechanism: A molecular rationale for the therapeutic application of iron chelators in human diseases involving the 2-oxoacid utilizing dioxygenases. *Curr. Med. Chem. 10*, 1005–1019.
10. Hanauske-Abel, H. M., and Günzler, V. (1982) A stereochemical concept for the catalytic mechanism of prolylhydroxylase. Applicability to classification and design of inhibitors. *J. Theor. Biol. 94*, 421–455.
11. Price, J. C., Barr, E. W., Tirupati, B., Bollinger, J. M.Jr., and Krebs, C. (2003) The first direct characterization of a high-valent iron intermediate in the reaction of an α-ketoglutarate-dependent dioxygenase: A high-spin Fe(IV) complex in taurine/α-ketoglutarate dioxygenase (TauD) from *Escherichia coli*. *Biochemistry 42*, 7497–7508.
12. Hoffart, L. M., Barr, E. W., Guyer, R. B., Bollinger, J. M.Jr., and Krebs, C. (2006) Direct spectroscopic detection of a C-H-cleaving high-spin Fe(IV) complex in a prolyl-4-hydroxylase. *Proc. Natl. Acad. Sci. U.S.A. 103*, 14738–14743.
13. Price, J. C., Barr, E. W., Glass, T. E., Krebs, C., and Bollinger, J. M.Jr. (2003) Evidence for hydrogen abstraction from C1 of taurine by the high-spin Fe(IV) intermediate detected during oxygen activation by taurine:α-ketoglutarate dioxygenase (TauD). *J. Am. Chem. Soc. 125*, 13008–13009.
14. Proshlyakov, D. A., Henshaw, T. F., Monterosso, G. R., Ryle, M. J., and Hausinger, R. P. (2004) Direct detection of oxygen intermediates in the non-heme Fe enzyme taurine/α-ketoglutarate dioxygenase. *J. Am. Chem. Soc. 126*, 1022–1023.
15. Riggs-Gelasco, P. J., Price, J. C., Guyer, R. B., Brehm, J. H., Barr, E. W., Bollinger, J. M.Jr., and Krebs, C. (2004) EXAFS spectroscopic evidence for an Fe=O unit in the Fe(IV) intermediate observed during oxygen activation by taurine:α-ketoglutarate dioxygenase. *J. Am. Chem. Soc. 126*, 8108–8109.
16. Groves, J. T. (1985) Key elements of the chemistry of cytochrome P-450. The oxygen rebound mechanism. *J. Chem. Educ. 62*, 9928–9931.
17. Vaillancourt, F. H., Yin, J., and Walsh, C. T. (2005) SyrB2 in syringomycin E biosynthesis is a nonheme Fe^{II} α-ketoglutarate- and O_2-dependent halogenase. *Proc. Natl. Acad. Sci. U.S.A. 102*, 10111–10116.
18. Vaillancourt, F. H., Vosburg, D. A., and Walsh, C. T. (2006) Dichlorination and bromination of a threonyl-*S*-carrier protein by the non-heme Fe(II) halogenase SyrB2. *ChemBioChem 7*, 748–752.
19. Galonić, D. P., Vaillancourt, F. H., and Walsh, C. T. (2006) Halogenation of unactivated carbon centers in natural product biosynthesis: Trichlorination of leucine during barbamide biosynthesis. *J. Am. Chem. Soc. 128*, 3900–3901.
20. Vaillancourt, F. H., Yeh, E., Vosburg, D. A., O'Connor, S. E., and Walsh, C. T. (2005) Cryptic chlorination by a non-haem iron enzyme during cyclopropyl amino acid biosynthesis. *Nature 436*, 1191–1194.
21. Vaillancourt, F. H., Yeh, E., Vosburg, D. A., Garneau-Tsodikova, S., and Walsh, C. T. (2006) Nature's inventory of halogenation catalysts: Oxidative strategies predominate. *Chem. Rev. 106*, 3364–3378.
22. Blasiak, L. C., Vaillancourt, F. H., Walsh, C. T., and Drennan, C. L. (2006) Crystal structure of the non-haem iron halogenase SyrB2 in syringomycin biosynthesis. *Nature 440*, 368–371.
23. Galonić, D. P., Barr, E. W., Walsh, C. T., Bollinger, J. M.Jr., and Krebs, C. (2007) Two interconverting Fe(IV) intermediates in aliphatic chlorination by the halogenase CytC3. *Nat. Chem. Biol. 3*, 113–116.
24. Galonić Fujimori, D., Barr, E. W., Matthews, M. L., Koch, G. M., Yonce, J. R., Walsh, C. T., Bollinger, J. M.Jr., Krebs, C., and Riggs-Gelasco, P. J. (2007) Spectroscopic evidence for a high-spin Br-Fe(IV)-oxo intermediate in the α-ketoglutarate-dependent halogenase CytC3 from *Streptomyces*. *J. Am. Chem. Soc. 129*, 13408–13409.
25. Grzyska, P. K., Ryle, M. J., Monterosso, G. R., Liu, J., Ballou, D. P., and Hausinger, R. P. (2005) Steady-state and transient kinetic analyses of taurine/α-ketoglutarate dioxygenase: Effects of oxygen concentration, alternative sulfonates, and active-site variants on the Fe(IV)-oxo intermediate. *Biochemistry 44*, 3845–3855.
26. Bollinger, J. M.Jr., and Krebs, C. (2006) Stalking intermediates in oxygen activation by iron enzymes: Motivation and method. *J. Inorg. Biochem. 100*, 586–605.
27. Zhou, J., Kelly, W. L., Bachmann, B. O., Gunsior, M., Townsend, C. A., and Solomon, E. I. (2001) Spectroscopic studies of substrate interactions with clavaminate synthase 2, a multifunctional α-KG-dependent non-heme iron enzyme: Correlation with mechanisms and reactivities. *J. Am. Chem. Soc. 123*, 7388–7398.
28. Bollinger, J. M.Jr., Tong, W. H., Ravi, N., Huynh, B. H., Edmondson, D. E., and Stubbe, J. (1994) Mechanism of assembly of the tyrosyl radical-diiron(III) cofactor of *E. coli* ribonucleotide reductase. 2. Kinetics of the excess Fe^{2+} reaction by optical, EPR, and Mössbauer spectroscopies. *J. Am. Chem. Soc. 116*, 8015–8023.
29. Ueki, M., Galonić, D. P., Vaillancourt, F. H., Garneau-Tsodikova, S., Yeh, E., Vosburg, D. A., Schroeder, F. C., Osada, H., and Walsh, C. T. (2006) Enzymatic generation of the antimetabolite γ,γ-dichloroaminobutyrate by NRPS and mononuclear iron halogenase action in a streptomycete. *Chem. Biol. 13*, 1183–1191.
30. Quadri, L. E. N., Weinreb, P. H., Lei, M., Nakano, M. M., Zuber, P., and Walsh, C. T. (1998) Characterization of Sfp, a *Bacillus subtilis* phosphopantetheinyl transferase for peptidyl carrier protein domains in peptide synthetases. *Biochemistry 37*, 1585–1595.
31. Gill, S. C., and von Hippel, P. H. (1989) Calculation of protein extinction coefficients from amino acid sequence data. *Anal. Biochem. 182*, 319–326.
32. Trauger, J. W., Kohli, R. M., Mootz, H. D., Marahiel, M. A., and Walsh, C. T. (2000) Peptide cyclization catalysed by the thioesterase domain of tyrocidine synthetase. *Nature 407*, 215–218.
33. Bollinger, J. M.Jr., Tong, W. H., Ravi, N., Huynh, B. H., Edmondson, D. E., and Stubbe, J. A. (1995) Use of rapid kinetics methods to study the assembly of the diferric-tyrosyl radical cofactor of *E. coli* ribonucleotide reductase. *Methods Enzymol. 258*, 278–303.
34. Price, J. C., Barr, E. W., Hoffart, L. M., Krebs, C., and Bollinger, J. M.Jr. (2005) Kinetic dissection of the catalytic mechanism of taurine:α-ketoglutarate dioxygenase (TauD) from *Escherichia coli*. *Biochemistry 44*, 8138–8147.
35. Younker, J. M., Krest, C. M., Jiang, W., Krebs, C., Bollinger, J. M. Jr., and Green, M. T. (2008) Structural analysis of the Mn(IV)/Fe(III) cofactor of *Chlamydia trachomatis* ribonucleotide reductase by extended X-ray absorption fine structure spectroscopy and density functional theory calculations. *J. Am. Chem. Soc. 130*, 15022–15027.
36. Ankoudinov, A. L. (1996) *Relativistic spin-dependent X-ray absorption theory*, University of Washington, Seattle.
37. *Gaussian 03*, revision E.01 (2003) Gaussian, Inc., Pittsburgh, PA.
38. Ehmann, D. E., Trauger, J. W., Stachelhaus, T., and Walsh, C. T. (2000) Aminoacyl-SNACs as small-molecule substrates for the condensation domains of nonribosomal peptide synthetases. *Chem. Biol. 7*, 765–772.
39. Kling, E., Schmid, C., Unversucht, S., Wage, T., Zehner, S., and van Pée, K. H. (2005) Enzymatic incorporation of halogen atoms into natural compounds. *Ernst Schering Res. Found. Workshop,* 165–194.
40. Hatcher, E., Soudackov, A. V., and Hammes-Schiffer, S. (2007) Proton-coupled electron transfer in soybean lipoxygenase: Dynamical behavior and temperature dependence of kinetic isotope effects. *J. Am. Chem. Soc. 129*, 187–196.
41. Eser, B. E., Barr, E. W., Frantom, P. A., Saleh, L., Bollinger, J. M.Jr., Krebs, C., and Fitzpatrick, P. F. (2007) Direct spectroscopic evidence for a high-spin Fe(IV) intermediate in tyrosine hydroxylase. *J. Am. Chem. Soc. 129*, 11334–11335.
42. Kaizer, J., Klinker, E. J., Oh, N. Y., Rohde, J.-U., Song, W. J., Stubna, A., Kim, J., Münck, E., Nam, W., and Que, L.Jr. (2004) Nonheme Fe(IV)O complexes that can oxidize the C-H bonds of cyclohexane at room temperature. *J. Am. Chem. Soc. 126*, 472–473.
43. Ryle, M. J., Liu, A., Muthukumaran, R. B., Ho, R. Y., Koehntop, K. D., McCracken, J., Que, L.Jr., and Hausinger, R. P. (2003) O_2- and

α-ketoglutarate-dependent tyrosyl radical formation in TauD, an α-keto acid-dependent non-heme iron dioxygenase. *Biochemistry 42*, 1854–1862.
44. Luo, Y.-R. (2007) *Comprehensive handbook of chemical bond energies*, CRC Press Inc., Boca Raton, FL.
45. Penner-Hahn, J. E., and Hodgson, K. O. (1989) X-ray Absorption Spectroscopy of Iron Porphyrins. In *Physical Bioinorganic Chemistry* (Lever, A. B. P., and Gray, H. B., Eds.) VCH Publishers, New York.
46. Rohde, J.-U., Torelli, S., Shan, X., Lim, M. H., Klinker, E. J., Kaizer, J., Chen, K., Nam, W., and Que, L.Jr. (2004) Structural insights into nonheme alkylperoxoiron(III) and oxoiron(IV) intermediates by X-ray absorption spectroscopy. *J. Am. Chem. Soc. 126*, 16750–16761.
47. Rohde, J.-U., Stubna, A., Bominaar, E. L., Münck, E., Nam, W., and Que, L.Jr. (2006) Nonheme oxoiron(IV) complexes of tris(2-pyridylmethyl)amine with *cis*-monoanionic ligands. *Inorg. Chem. 45*, 6435–6445.